

Supporting Information

for

Synthesis, Characterization and Photoinduced CO-Release by Manganese(I) Complexes

André L. Amorim^{a,†}, Ana Guerreiro^{b,†}, Vinícius A. Glitz^a, Daniel F. Coimbra^a, Adailton J. Bortoluzzi^a, Giovanni F. Caramori^a, Antonio L. Braga^a, Ademir Neves^a, Gonçalo J. L. Bernardes^{b,c,*} and Rosely A. Peralta^{a,*}

[^a] Departamento de Química, Universidade Federal de Santa Catarina, Florianópolis, Santa Catarina 88040-900, Brazil

[^b] Instituto de Medicina Molecular, Faculdade de Medicina, Universidade de Lisboa, Avenida Professor Egas Moniz, 1649-028, Lisboa (Portugal)

[^c] Department of Chemistry, University of Cambridge, Lensfield Road, Cambridge CB2 1EW (UK)

[†]These authors contributed equally to this work.

List of Figures

Figure S1. ATR infrared spectrum for 1	5
Figure S2. ATR infrared spectrum for 2	5
Figure S3. ATR infrared spectrum for 3	6
Figure S4. ATR infrared spectrum for 4	6
Figure S5. Shifts in the normalized UV spectrum of 2 in dichloromethane (solid line) and acetonitrile initial (dashed line) and after 12 h incubation (dotted line).....	7
Figure S6. Shifts in the normalized UV spectrum of 3 in dichloromethane (solid line) and acetonitrile initial (dashed line) and after 12 h incubation (dotted line).....	7
Figure S7. Changes in the IR spectrum of 2 in dichloromethane (solid line) and acetonitrile (dashed line).	8
Figure S8. Changes in the IR spectrum of 3 in dichloromethane (solid line) and acetonitrile (dashed line).	8
Figure S9. Mass spectrum for 1 in CH ₃ CN, where the base peak is attributed to the fragment [Mn(CO) ₃ (dpa)] ⁺ (<i>m/z</i> = 338). Inset graph shows the superposition of the experimental (solid line) and predicted (dashed lines) spectrum.	9
Figure S10. Mass spectrum for 3_{py} in CH ₃ CN, where the base peak is attributed to the fragment [Mn(CO) ₃ (pmpea)] ⁺ (<i>m/z</i> = 352). Inset graph shows the superposition of the experimental (solid line) and predicted (dashed lines) spectra.	9
Figure S11. Mass spectrum for 4_{py} in CH ₃ CN, where the base peak is attributed to the fragment [Mn(CO) ₃ (bpea)] ⁺ (<i>m/z</i> = 366). Inset graph shows the superposition of the experimental (solid line) and predicted (dashed lines) spectra.	10
Figure S12. ¹ H NMR spectrum of 1 in CDCl ₃	10
Figure S13. ¹ H NMR spectrum of 3 in CDCl ₃	11
Figure S14. ¹ H NMR spectrum of 4 in CDCl ₃	11
Figure S15. The first five molecular orbitals (HOMO and LUMO) calculated for 1, 2, 2s, 3, 4 and 4py. The most prominent MOs involved in the transitions under lower energy band are shown.	12
Figure S16. Decrease in the UV absorption bands in dichloromethane for 1 over time during exposure to λ_{380} light. Inset shows the decrease in the 354 nm reference band over time.	13
Figure S17. Decrease in the UV absorption bands in acetonitrile for 1 over time during exposure to λ_{380} light. Inset shows the decrease in the 350 nm reference band over time.	13
Figure S18. Decrease in the UV absorption bands in dichloromethane for 2 over time during exposure to λ_{380} light. Inset shows the decrease in the 380 nm reference band over time.	14

Figure S19. Decrease in the UV absorption bands in acetonitrile for 2_s over time during exposure to λ_{380} light. Inset shows the decrease in the 363 nm reference band over time.....	14
Figure S20. Decrease in the UV absorption bands in dichloromethane for 3 over time during exposure to λ_{380} light. Inset shows the decrease in the 379 nm reference band over time.....	15
Figure S21. Decrease in the UV absorption bands in acetonitrile for 3_{py} over time during exposure to λ_{380} light. Inset shows the decrease in the 364 nm reference band over time.....	15
Figure S22. Decrease in the CO stretching bands in dichloromethane for 1 over time during exposure to λ_{380} light.....	16
Figure S23. Decrease in the CO stretching bands in acetonitrile for 1 over time during exposure to λ_{380} light.....	16
Figure S24. Decrease in the CO stretching bands in dichloromethane for 2 over time during exposure to λ_{380} light.....	17
Figure S25. Decrease in the CO stretching bands in dichloromethane for 3 over time during exposure to λ_{380} light.....	18
Figure S26. Decrease in the CO stretching bands in acetonitrile for 3_{py} over time during exposure to λ_{380} light.....	18
Figure S27. CO-release in aqueous solution. CO-release was measured (using COP-1) from 490 to 650 nm (lex=475 nm). Photoemission spectra were obtained at 0, 10, 20, 30, 40, 50, 60, 70, 80 and 90 min after the addition of 1 μ M COP-1 to 150 μ mol L ⁻¹ of either [Mn(CO) ₃ (dpa)]Br (1) (a), [MnBr(CO) ₃ (bpa)] (2) (b), [MnBr(CO) ₃ (pmpea)] (3) (c) or [MnBr(CO) ₃ (bpea)] (4) (d) in PBS pH 7.4 at 37°C. The results are shown as emission intensity in relative fluorescent units (RFUs) and were normalized to the control.	19
Figure S28. Cell viability after treatment with 1-4 . HeLa (a and b) and HepG2 (c and d) cells were incubated with several concentrations of 1-4 (1 μ mol L ⁻¹ , 5 μ mol L ⁻¹ , 10 μ mol L ⁻¹ , 25 μ mol L ⁻¹ , 50 μ mol L ⁻¹ , 100 μ mol L ⁻¹ and 150 μ mol L ⁻¹) for 24 h (left panel) and 48h (right panel) . 1 – green line, 2 - red line, 3 - blue line and 4 - yellow line. To measure cell viability, cells were incubated with CellTiter-Blue (Promega) for 90 min at 37°C after which the absorbance was measured. The results are shown as a percentage of the control.	20
Figure S29. Quantification of CO-release in live HeLa cells at 5, 30, 45 and 60 min after the addition of 1 μ M COP-1 in PBS pH 7.4 (lem = 497-558nm ,lex = 488 nm). Cells were previously incubated with either compound (1), (2) or (3) at 150 μ M. The results are shown as mean fluorescence intensity (arbitrary units) in relation to the cell-surface area, normalized to control (cells in the absence of compounds). The compounds (1) and (3) show a statistically significant increase in CO-release compared to the control at 45min ((1) P<0,0001; (2) P=0,0012) and at 60 min (P<0,0001), determined by a Mann Whitney test;	21

List of Tables

Table S1. Calculated and experimental CO stretching frequencies and the λ_{\max} for the proposed structures	23
Table S2. Selected bond lengths (in Å), where X is the atom in the position trans to a CO. Values inside parenthesis obtained from crystal structure data.....	23
Table S3. Crystal data and structure refinement for complex 1	24
Table S4. Bond lengths [Å] and angles [°] for complex 1	25
Table S5. Torsion angles [°] for complex 1	26
Table S6. Hydrogen bonds for complex 1 [Å and °].....	26
Table S7. Crystal data and structure refinement for complex 2	27
Table S8. Bond lengths [Å] and angles [°] for complex 2	28
Table S9. Torsion angles [°] for complex 2	28
Table S10. Crystal data and structure refinement for complex 3	29
Table S11. Bond lengths [Å] and angles [°] for complex 3	30
Table S12.. Torsion angles [°] for complex 3	31
Table S13. Hydrogen bonds for complex 3 [Å and °]	31

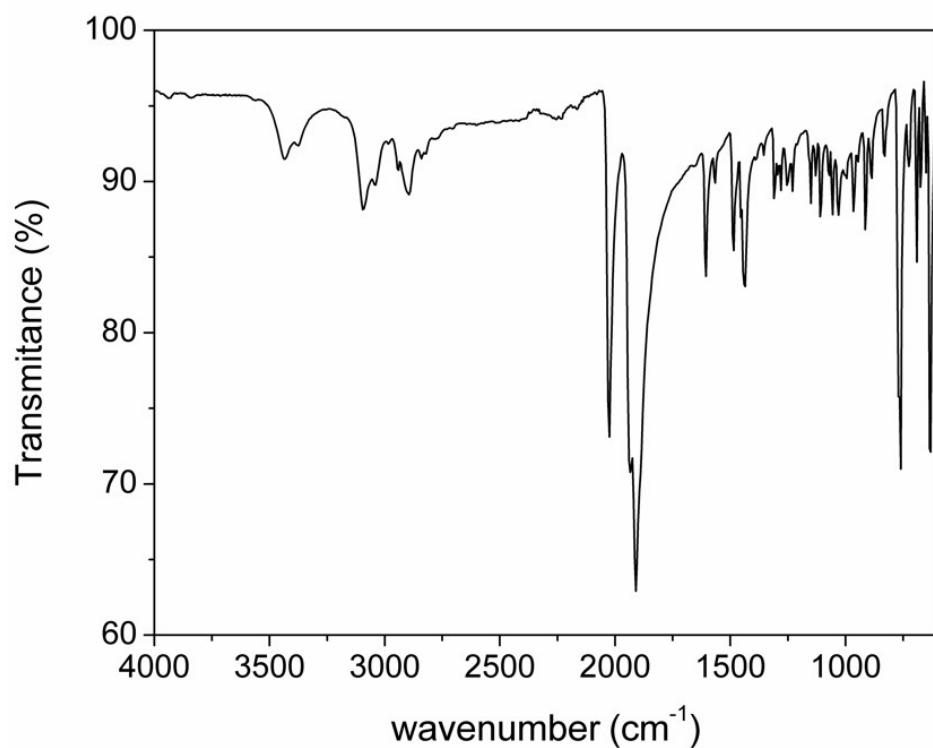


Figure S1. ATR infrared spectrum for **1**.

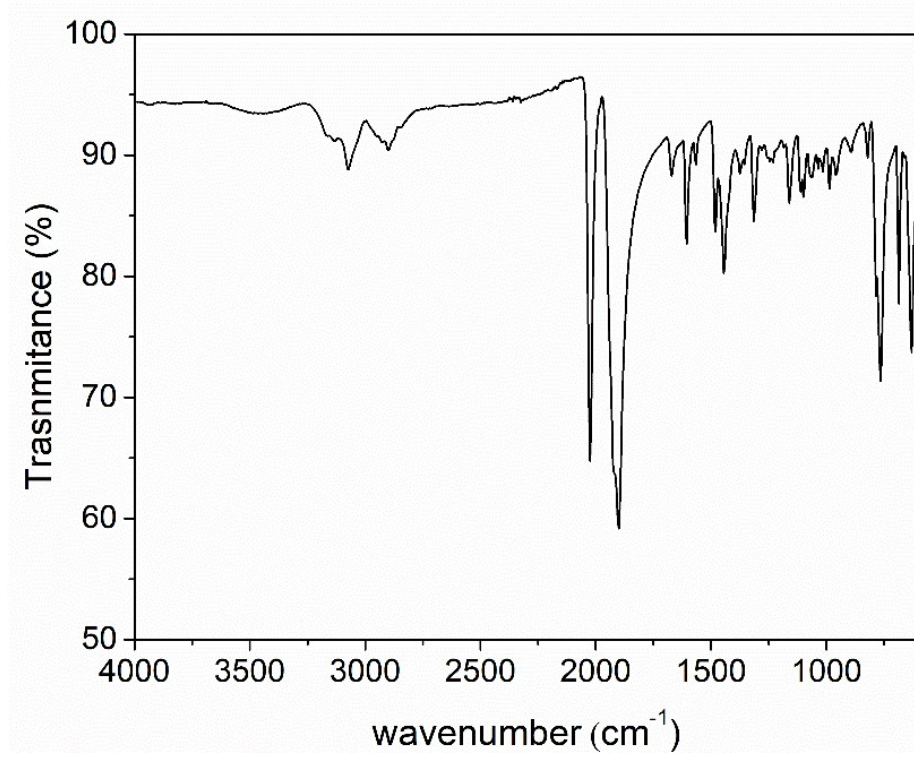


Figure S2. ATR infrared spectrum for **2**.

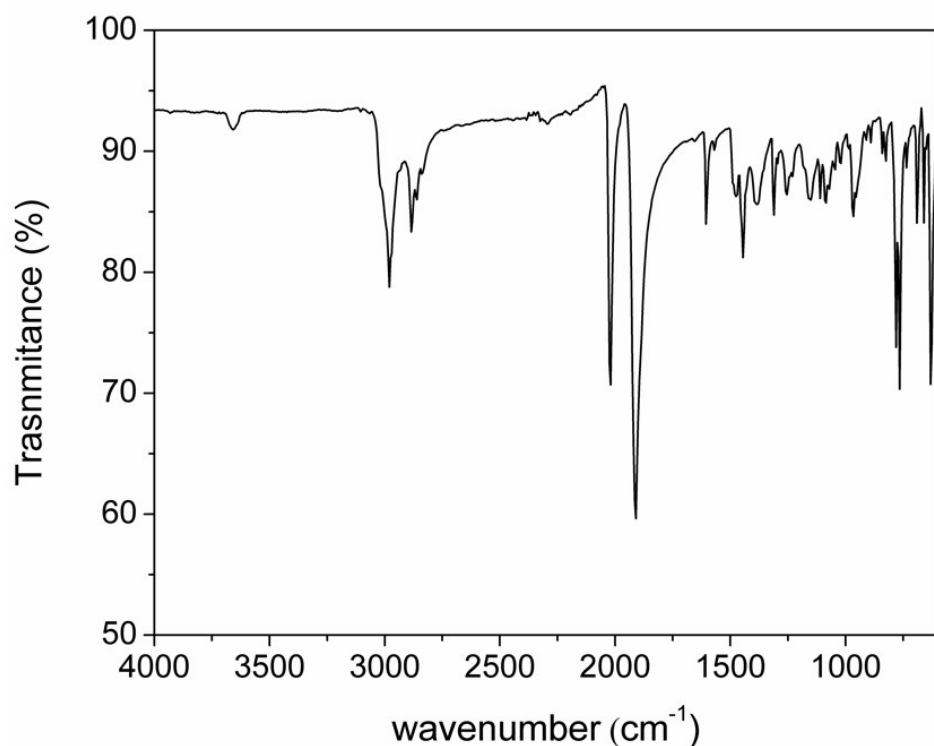


Figure S3. ATR infrared spectrum for **3**.

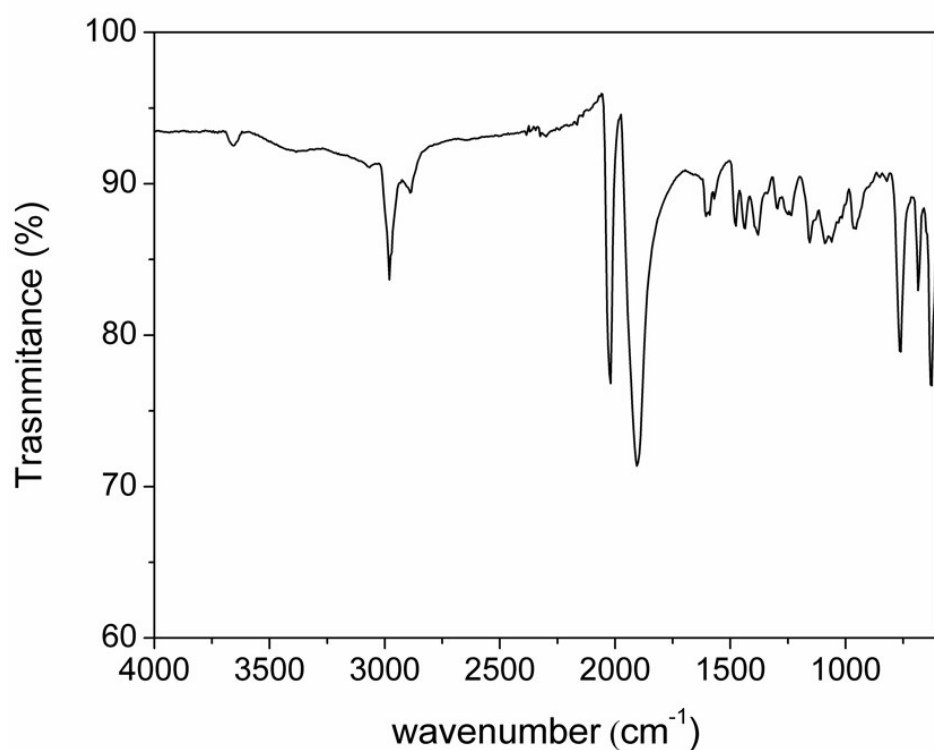


Figure S4. ATR infrared spectrum for **4**.

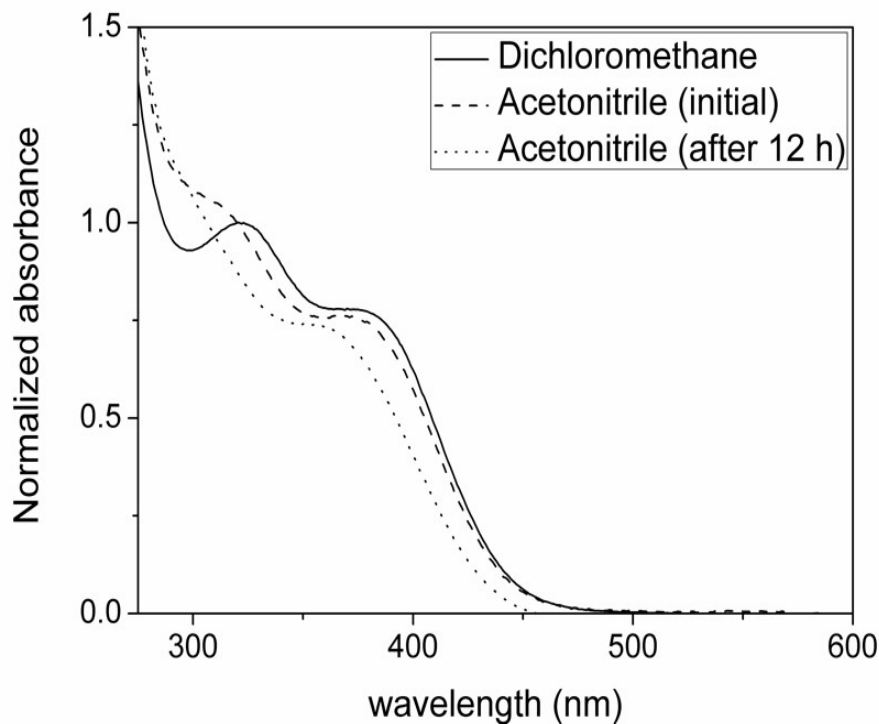


Figure S5. Shifts in the normalized UV spectrum of **2** in dichloromethane (solid line) and acetonitrile initial (dashed line) and after 12 h incubation (dotted line).

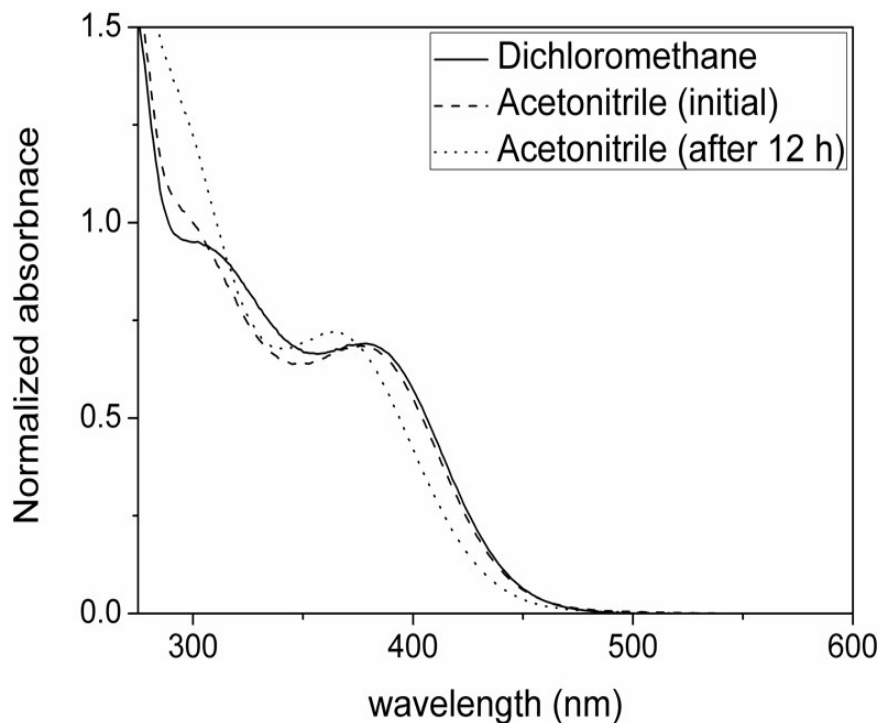


Figure S6. Shifts in the normalized UV spectrum of **3** in dichloromethane (solid line) and acetonitrile initial (dashed line) and after 12 h incubation (dotted line).

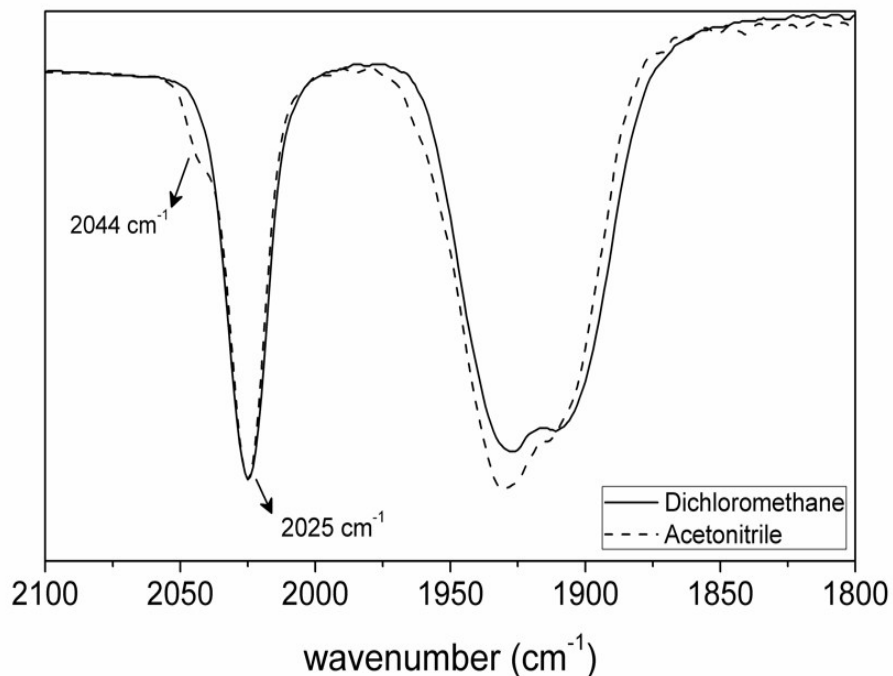


Figure S7. Changes in the IR spectrum of **2** in dichloromethane (solid line) and acetonitrile (dashed line).

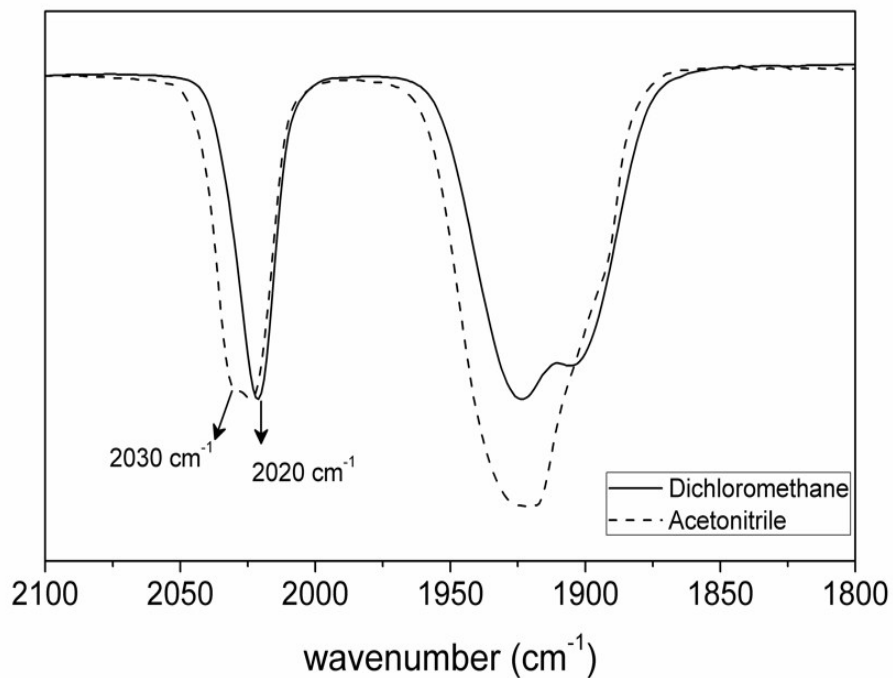


Figure S8. Changes in the IR spectrum of **3** in dichloromethane (solid line) and acetonitrile (dashed line).

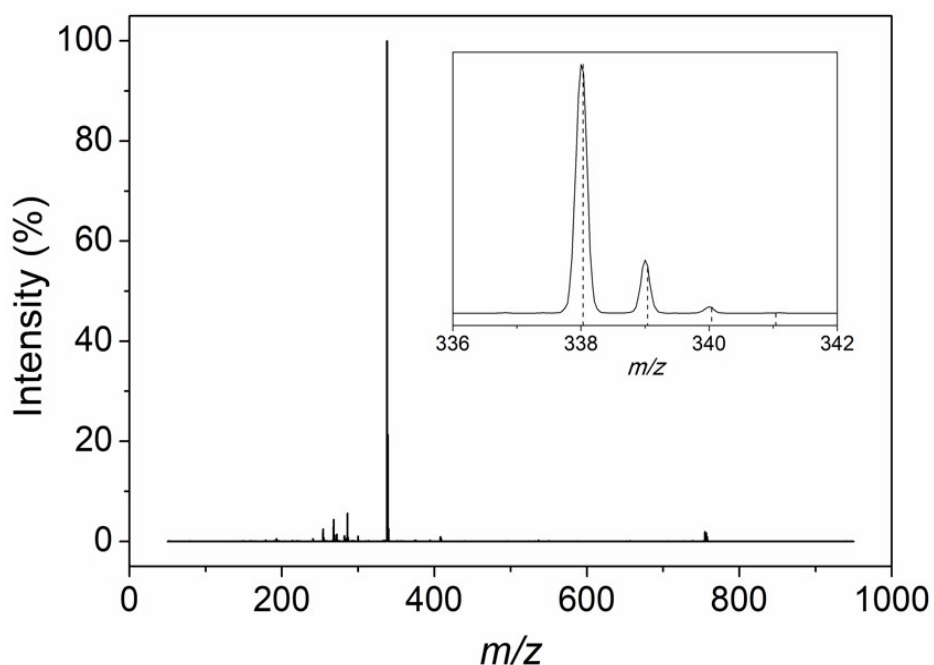


Figure S9. Mass spectrum for **1** in CH_3CN , where the base peak is attributed to the fragment $[\text{Mn}(\text{CO})_3(\text{dpa})]^+$ ($m/z = 338$). Inset graph shows the superposition of the experimental (solid line) and predicted (dashed lines) spectrum.

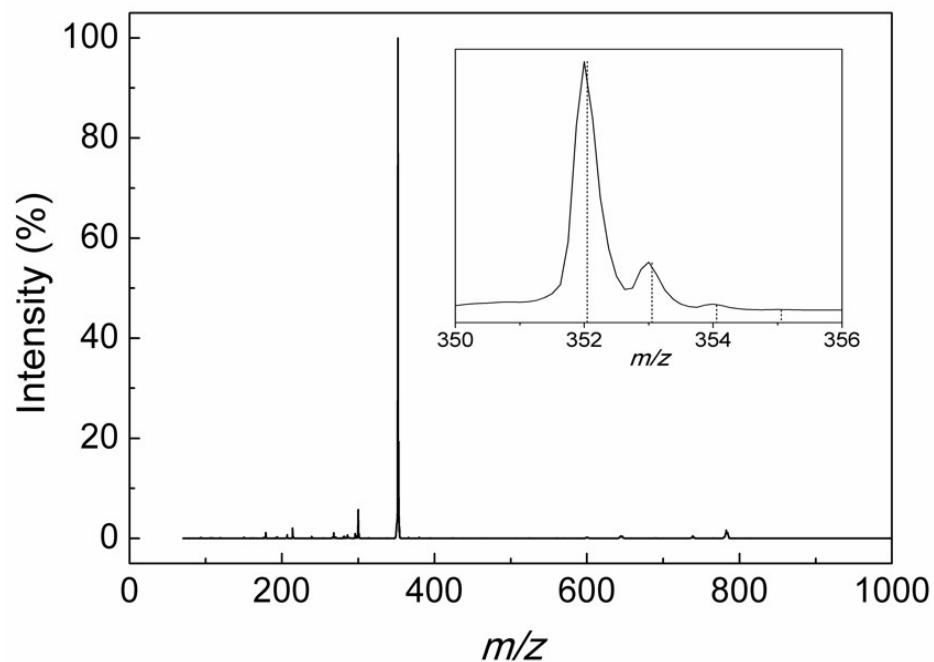


Figure S10. Mass spectrum for **3_{py}** in CH_3CN , where the base peak is attributed to the fragment $[\text{Mn}(\text{CO})_3(\text{pmpea})]^+$ ($m/z = 352$). Inset graph shows the superposition of the experimental (solid line) and predicted (dashed lines) spectra.

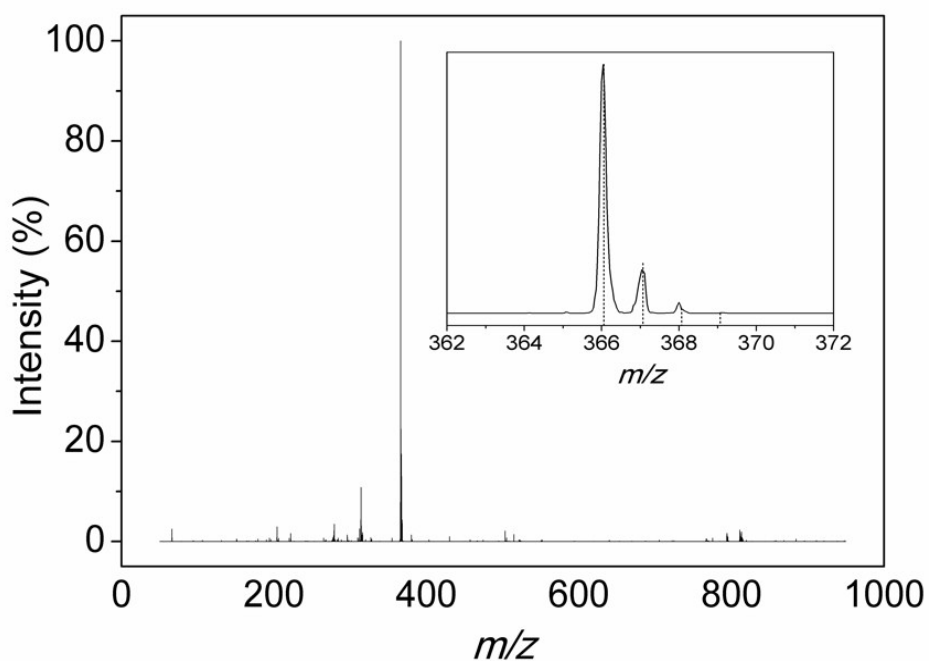


Figure S11. Mass spectrum for $\mathbf{4}_{\text{py}}$ in CH_3CN , where the base peak is attributed to the fragment $[\text{Mn}(\text{CO})_3(\text{bpea})]^+$ ($m/z = 366$). Inset graph shows the superposition of the experimental (solid line) and predicted (dashed lines) spectra.

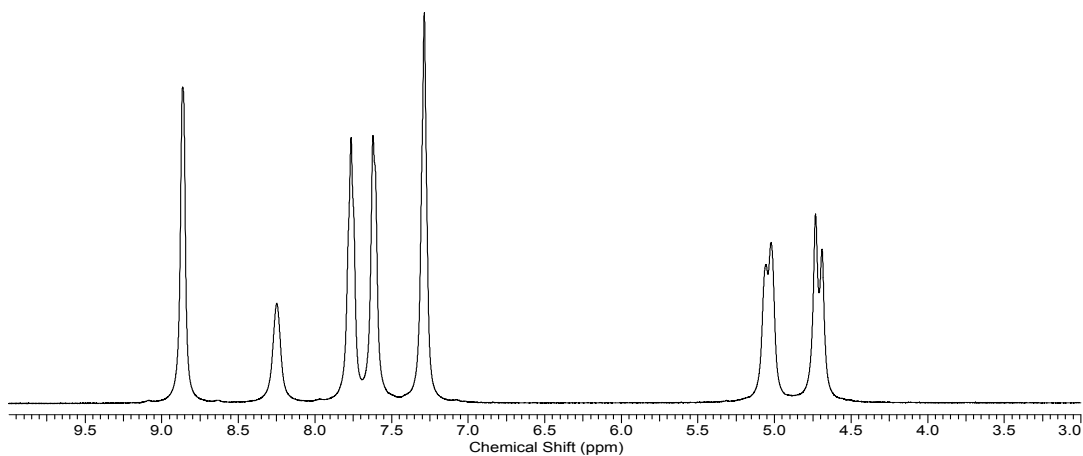


Figure S12. ^1H NMR spectrum of $\mathbf{1}$ in CDCl_3 .

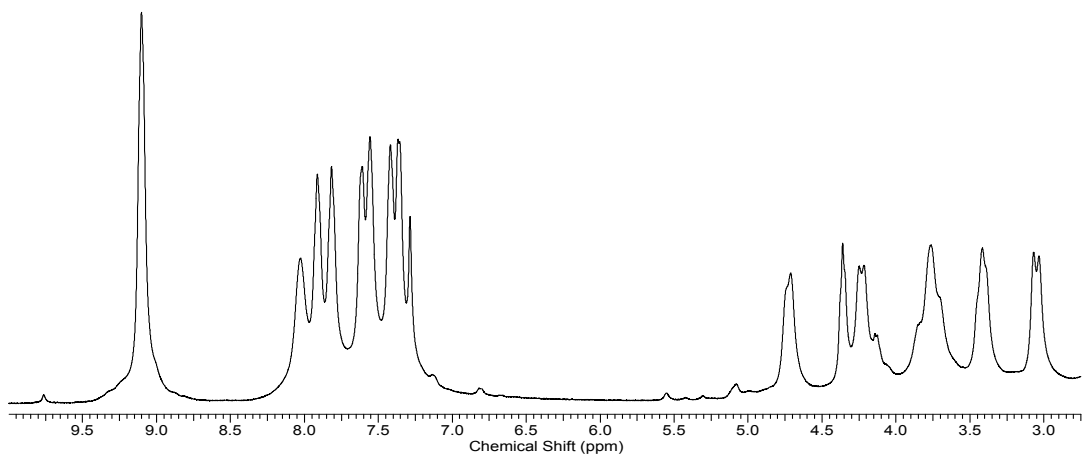


Figure S13. ¹H NMR spectrum of **3** in CDCl_3 .

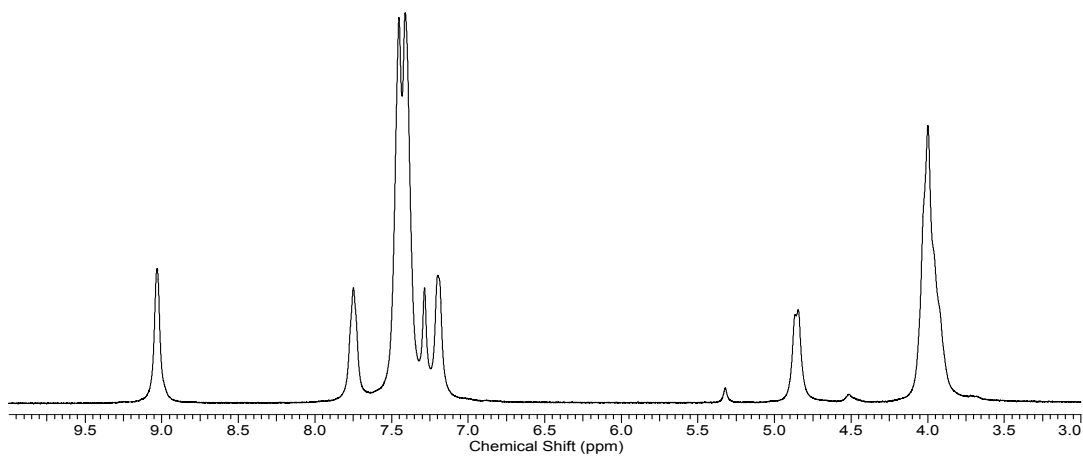


Figure S14. ¹H NMR spectrum of **4** in CDCl_3 .

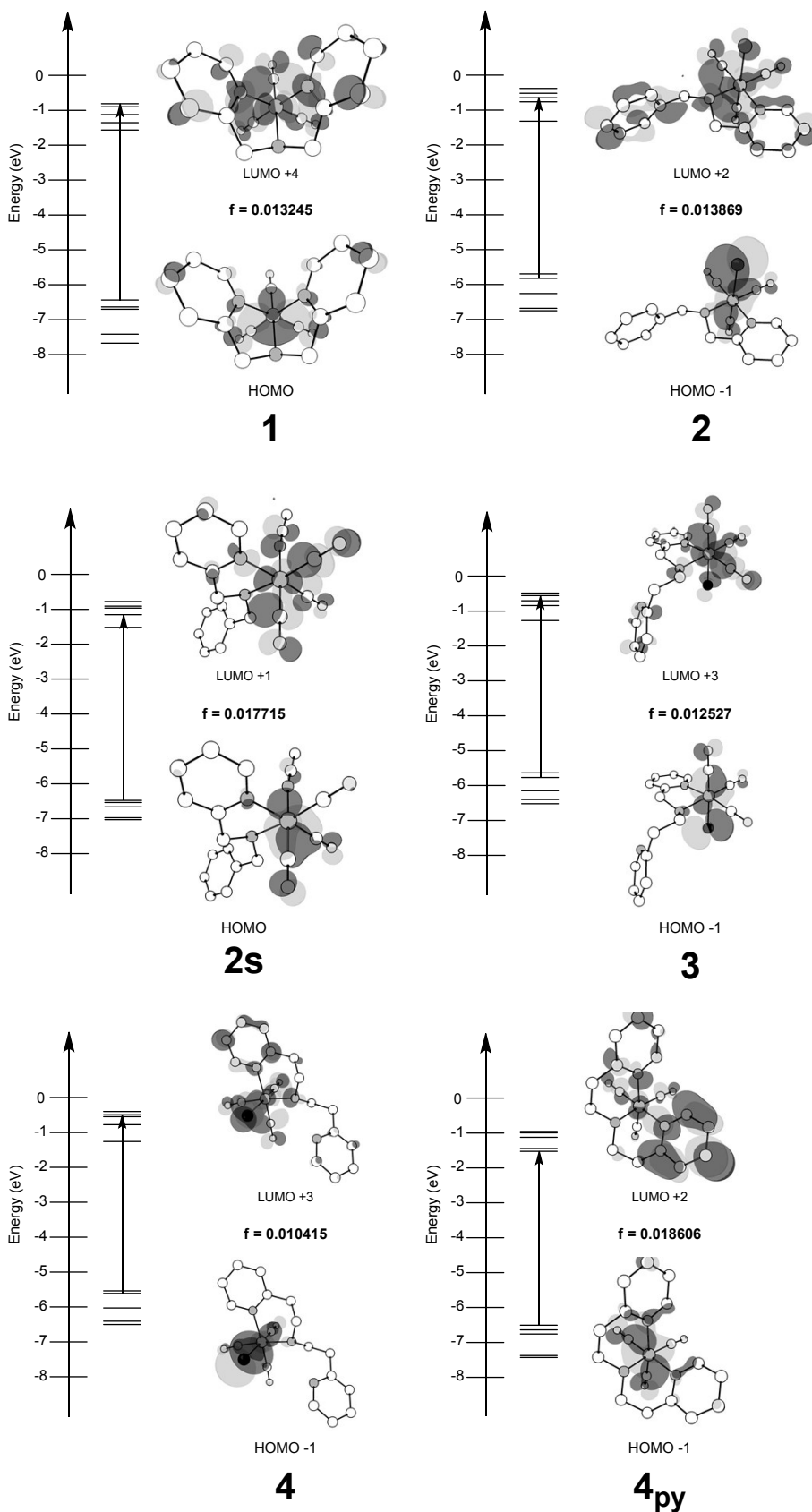


Figure S15. The first five molecular orbitals (HOMO and LUMO) calculated for 1, 2, 2s, 3, 4 and 4_{py}. The most prominent MOs involved in the transitions under lower energy band are shown.

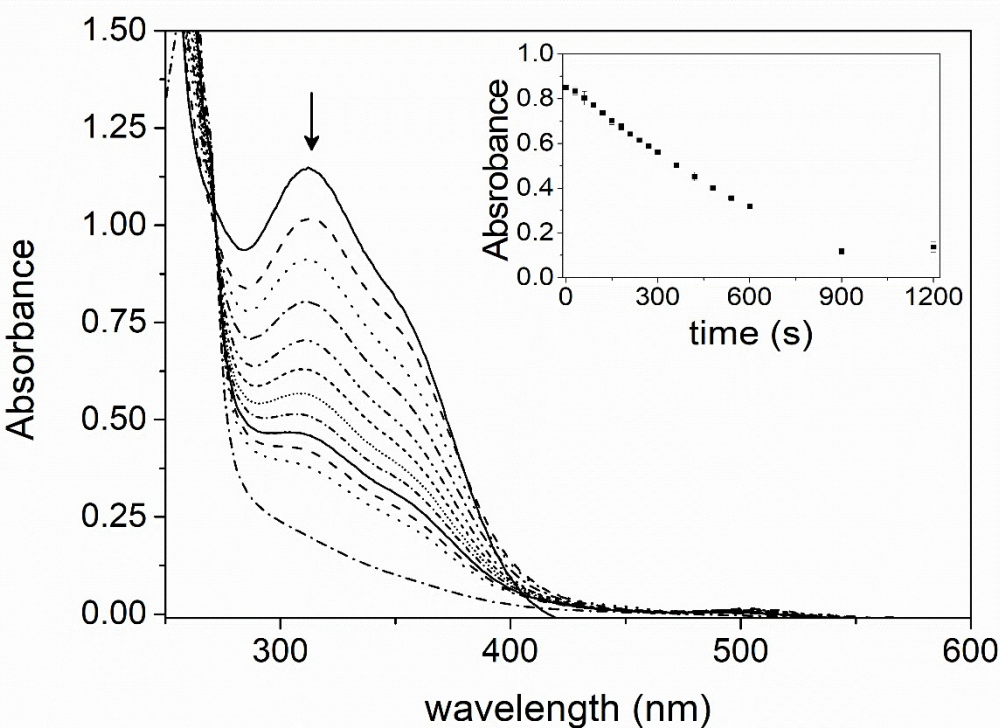


Figure S16. Decrease in the UV absorption bands in dichloromethane for **1** over time during exposure to λ_{380} light. Inset shows the decrease in the 354 nm reference band over time.

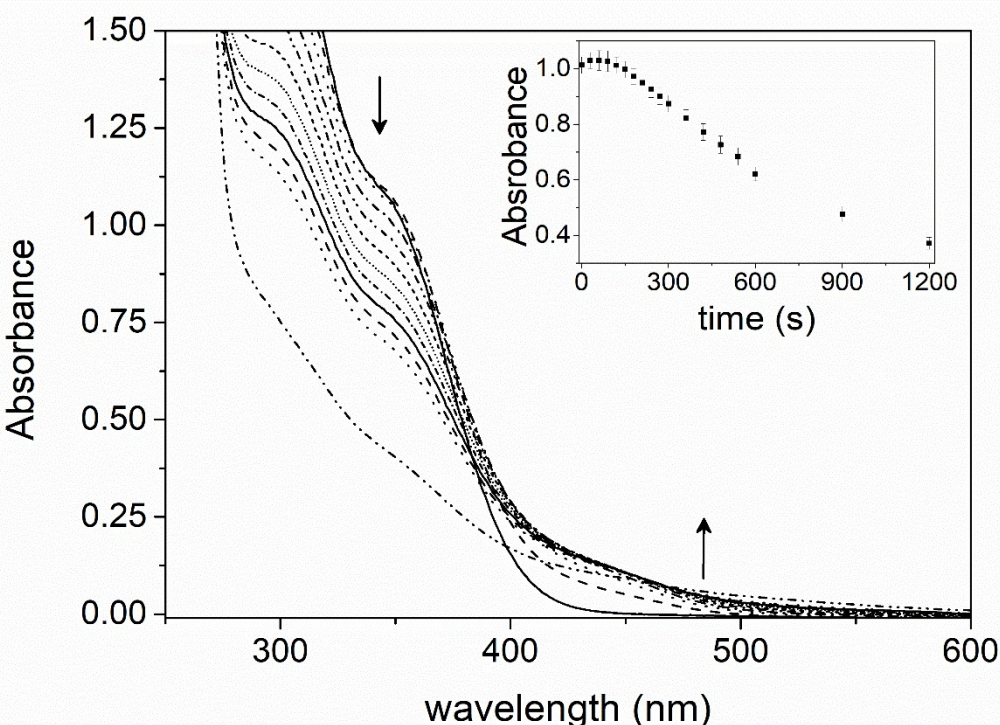


Figure S17. Decrease in the UV absorption bands in acetonitrile for **1** over time during exposure to λ_{380} light. Inset shows the decrease in the 350 nm reference band over time.

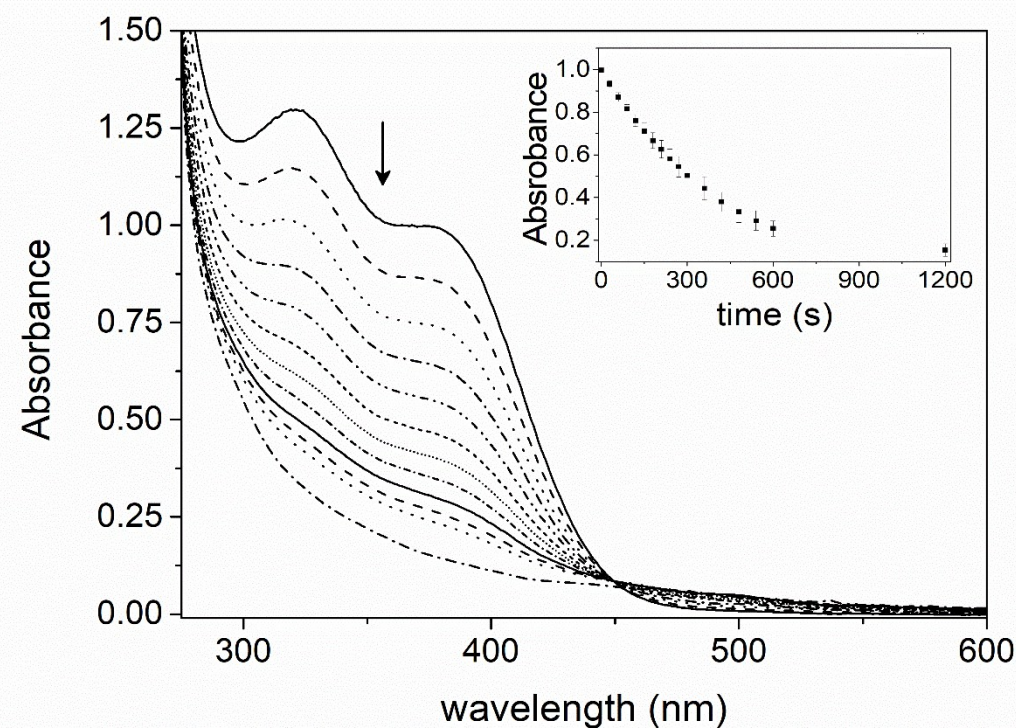


Figure S18. Decrease in the UV absorption bands in dichloromethane for **2** over time during exposure to λ_{380} light. Inset shows the decrease in the 380 nm reference band over time.

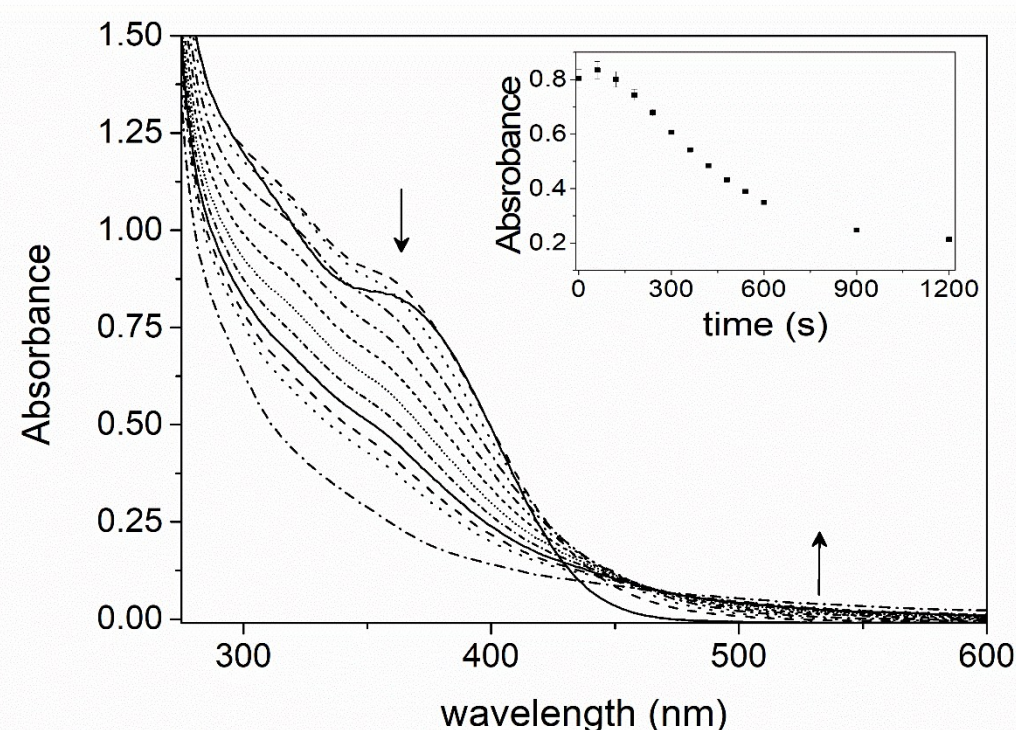


Figure S19. Decrease in the UV absorption bands in acetonitrile for **2s** over time during exposure to λ_{380} light. Inset shows the decrease in the 363 nm reference band over time.

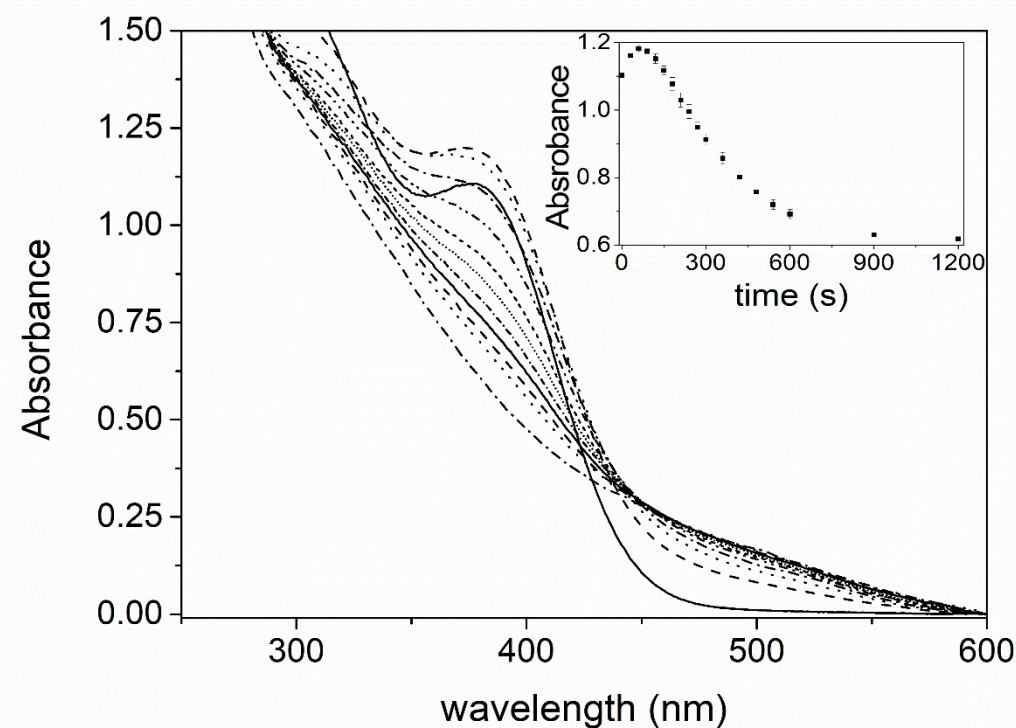


Figure S20. Decrease in the UV absorption bands in dichloromethane for **3** over time during exposure to λ_{380} light. Inset shows the decrease in the 379 nm reference band over time.

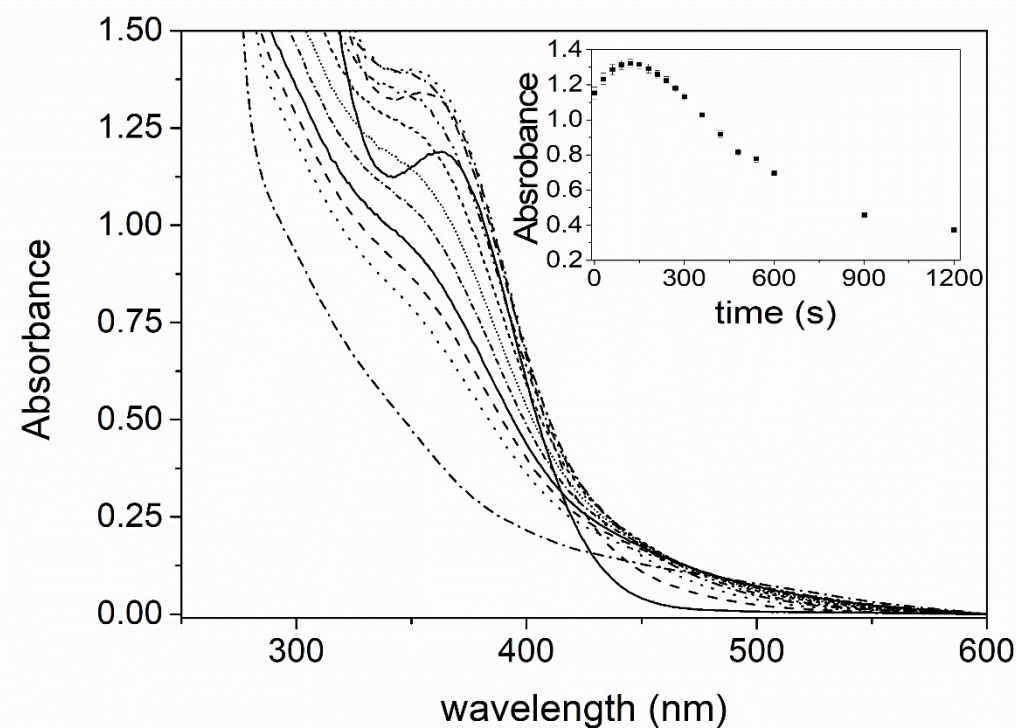


Figure S21. Decrease in the UV absorption bands in acetonitrile for **3_{py}** over time during exposure to λ_{380} light. Inset shows the decrease in the 364 nm reference band over time.

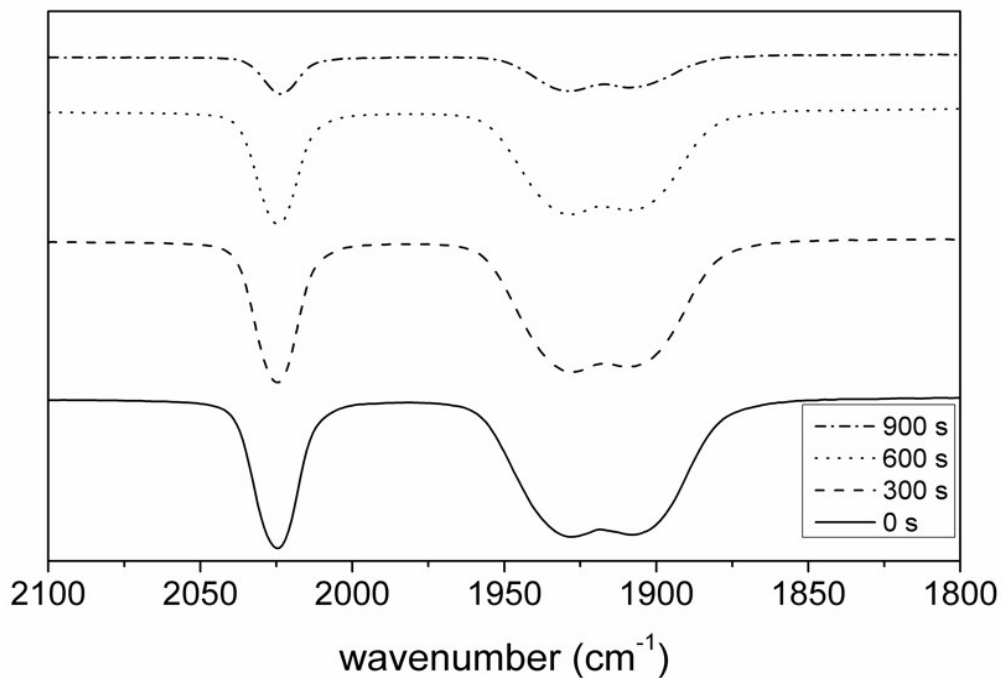


Figure S22. Decrease in the CO stretching bands in dichloromethane for **1** over time during exposure to λ_{380} light.

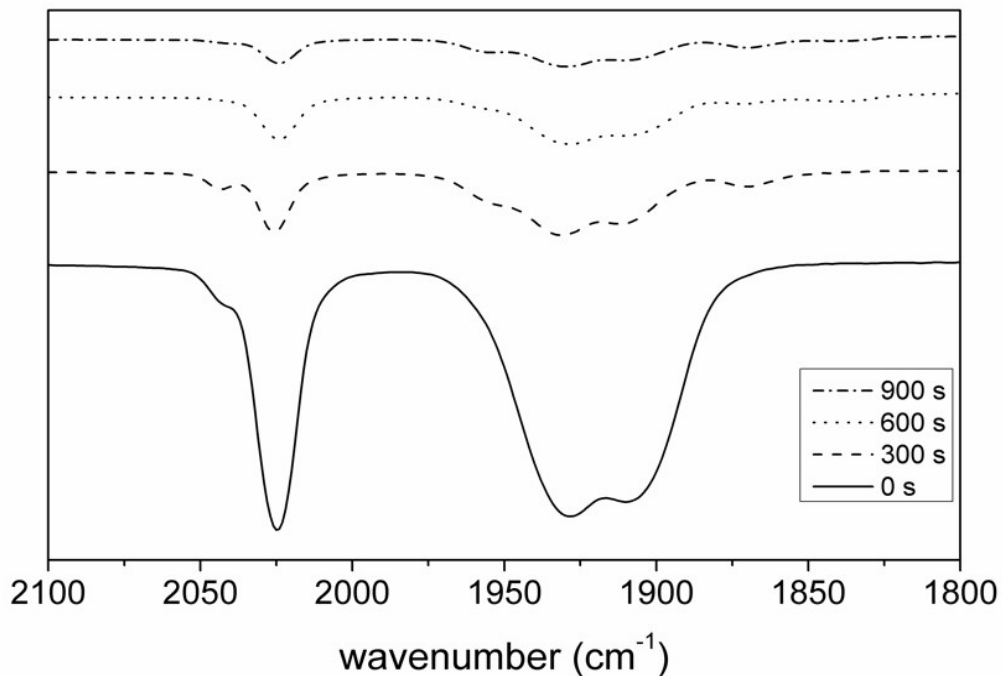


Figure S23. Decrease in the CO stretching bands in acetonitrile for **1** over time during exposure to λ_{380} light.

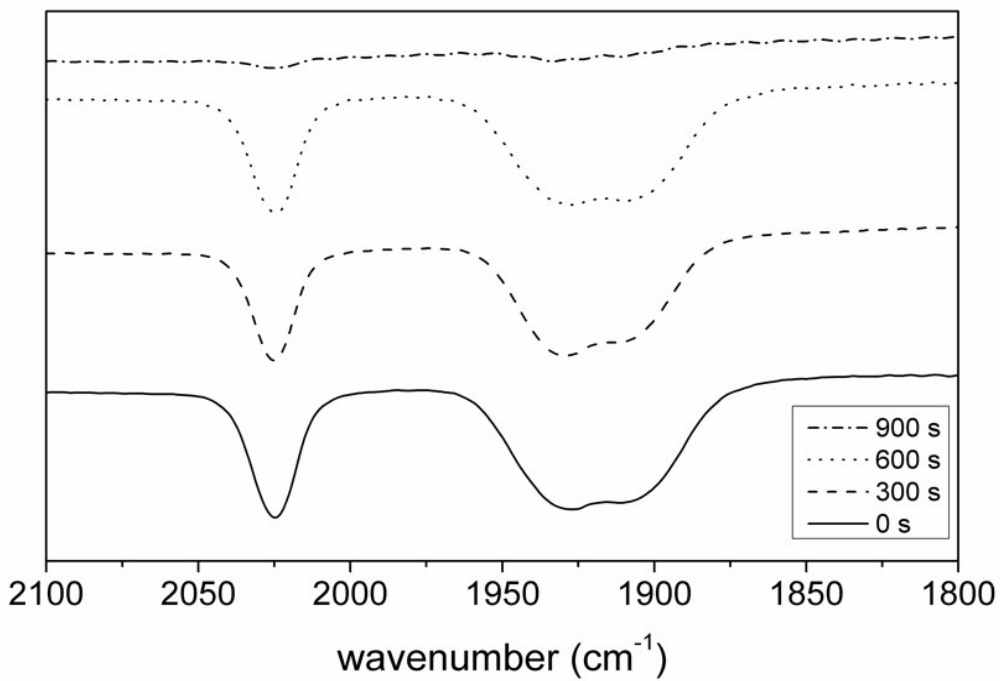


Figure S24. Decrease in the CO stretching bands in dichloromethane for **2** over time during exposure to λ_{380} light.

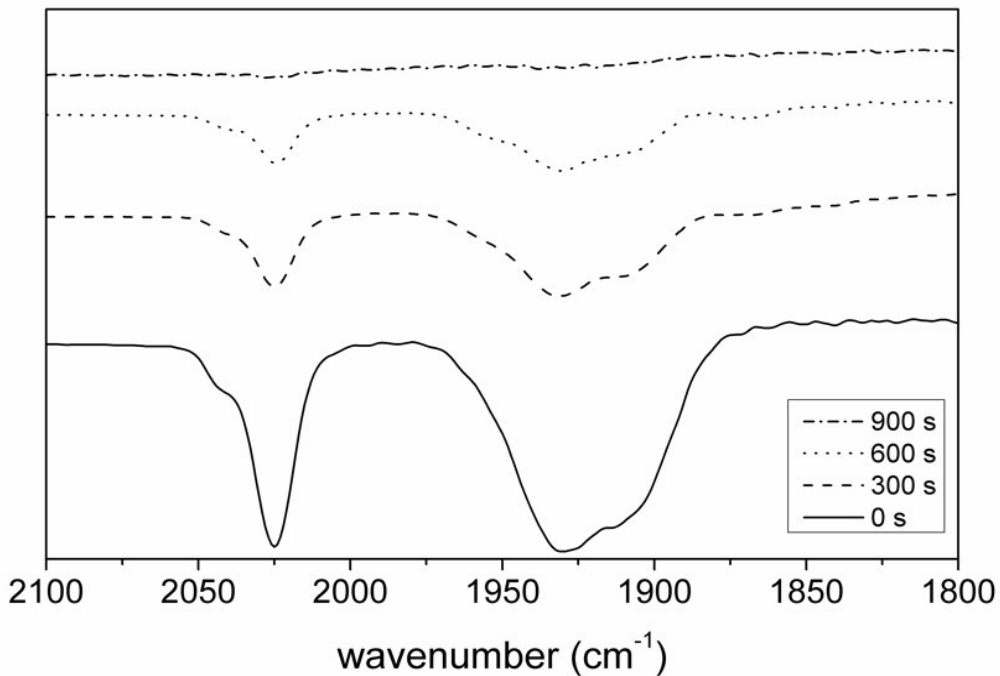


Figure S25. Decrease in the CO stretching bands in acetonitrile for **2**_s over time during exposure to λ_{380} light.

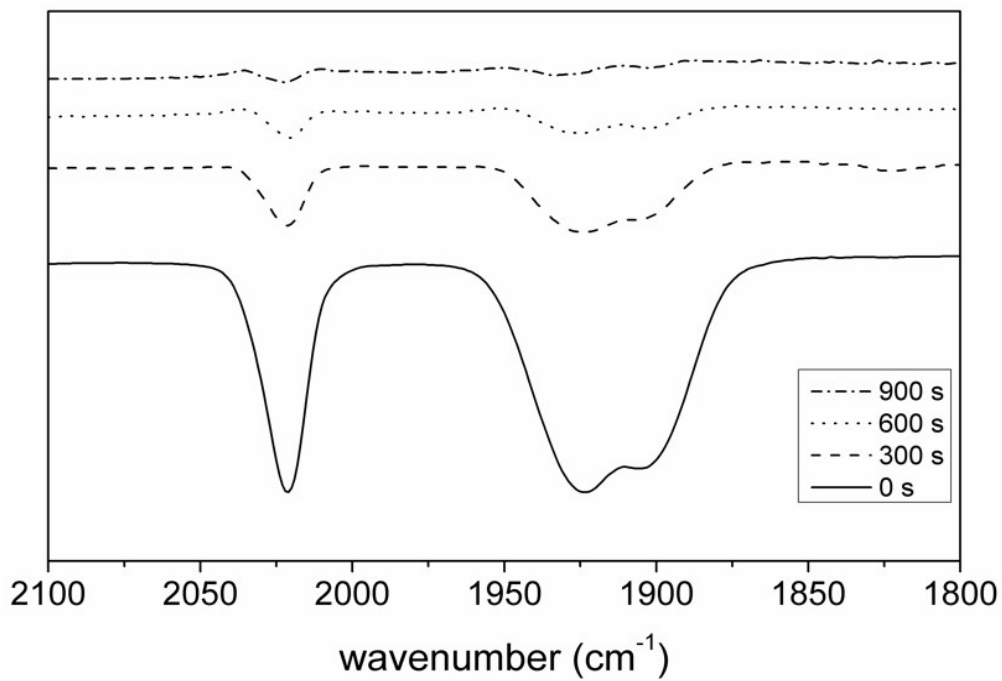


Figure S25. Decrease in the CO stretching bands in dichloromethane for **3** over time during exposure to λ_{380} light.

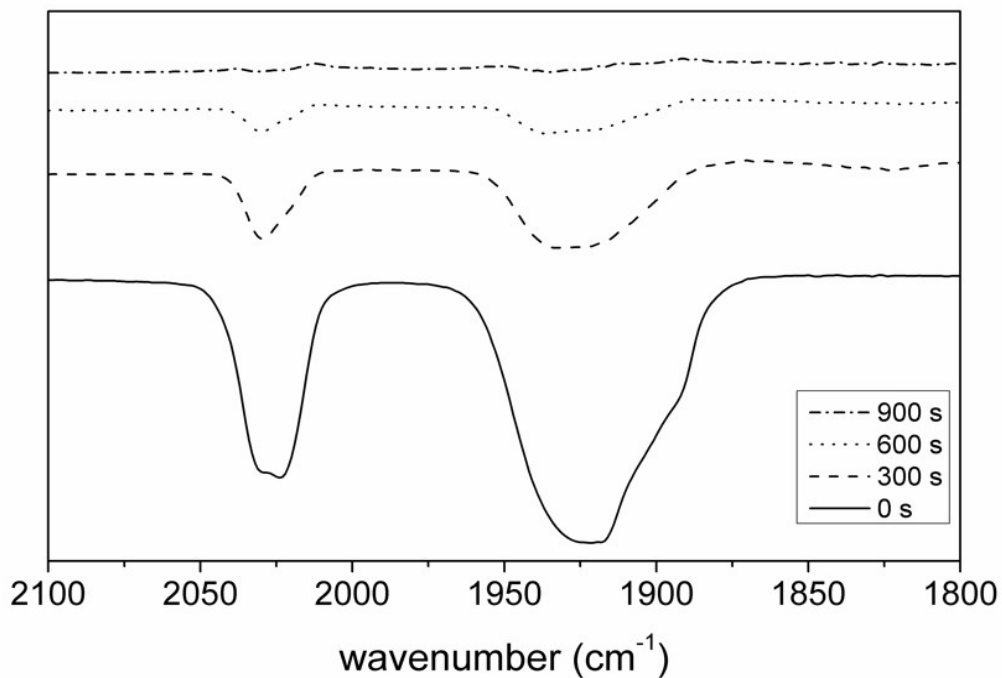


Figure S26. Decrease in the CO stretching bands in acetonitrile for **3_{py}** over time during exposure to λ_{380} light.

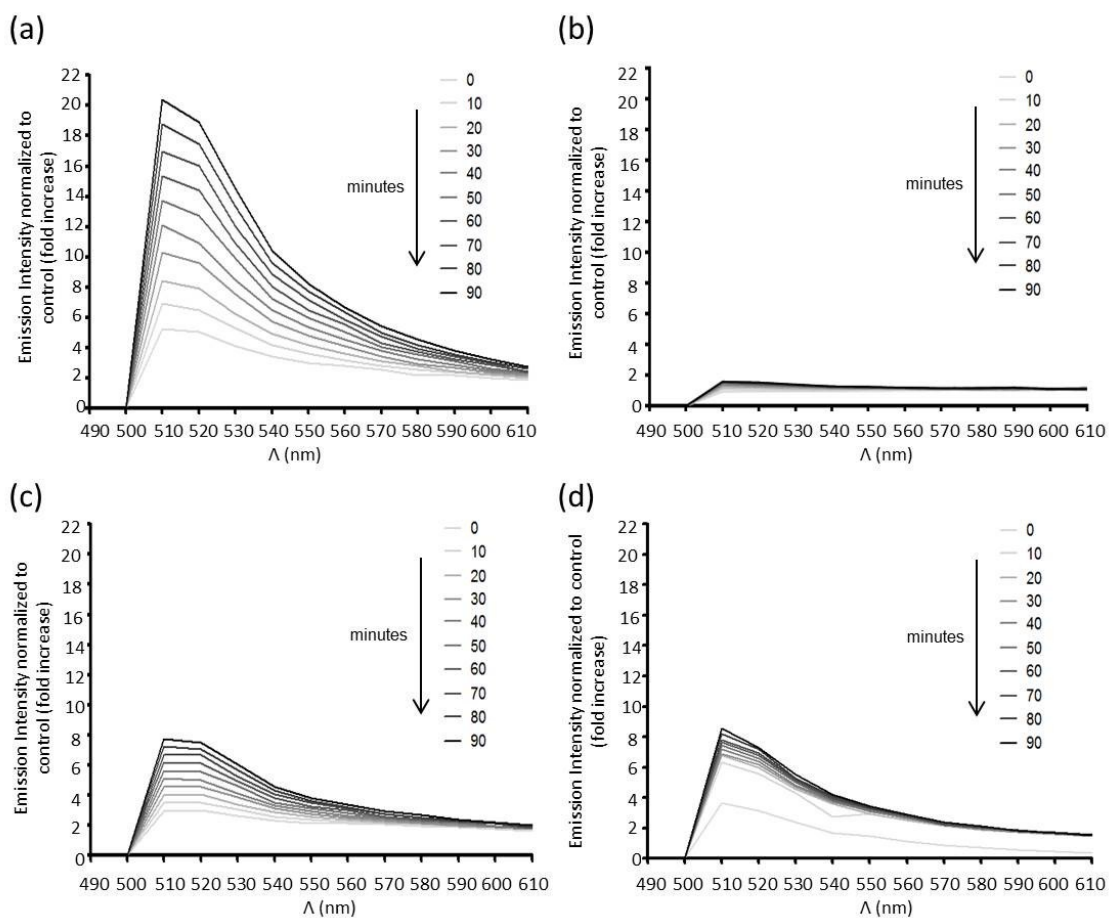


Figure S27. CO-release in aqueous solution. CO-release was measured (using COP-1) from 490 to 650 nm (lex=475 nm). Photoemission spectra were obtained at 0, 10, 20, 30, 40, 50, 60, 70, 80 and 90 min after the addition of 1 μ M COP-1 to 150 μ mol L⁻¹ of either [Mn(CO)₃(dpa)]Br (1) (a), [MnBr(CO)₃(bpa)] (2) (b), [MnBr(CO)₃(pmpea)] (3) (c) or [MnBr(CO)₃(bpea)] (4) (d) in PBS pH 7.4 at 37°C. The results are shown as emission intensity in relative fluorescent units (RFUs) and were normalized to the control.

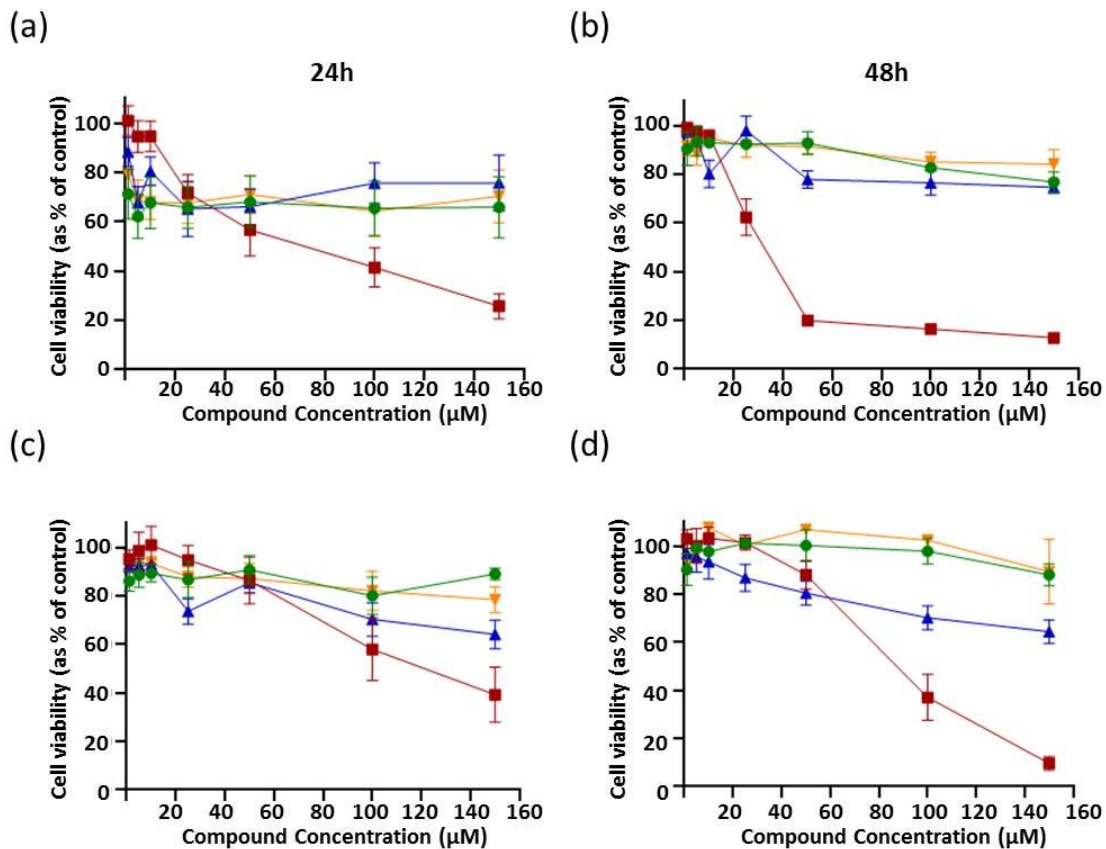


Figure S28. Cell viability after treatment with **1-4**. HeLa (a and b) and HepG2 (c and d) cells were incubated with several concentrations of **1-4** ($1 \mu\text{mol L}^{-1}$, $5 \mu\text{mol L}^{-1}$, $10 \mu\text{mol L}^{-1}$, $25 \mu\text{mol L}^{-1}$, $50 \mu\text{mol L}^{-1}$, $100 \mu\text{mol L}^{-1}$ and $150 \mu\text{mol L}^{-1}$) for 24 h (left panel) and 48h (right panel). **1** – green line, **2** - red line, **3** - blue line and **4** - yellow line. To measure cell viability, cells were incubated with CellTiter-Blue (Promega) for 90 min at 37°C after which the absorbance was measured. The results are shown as a percentage of the control.

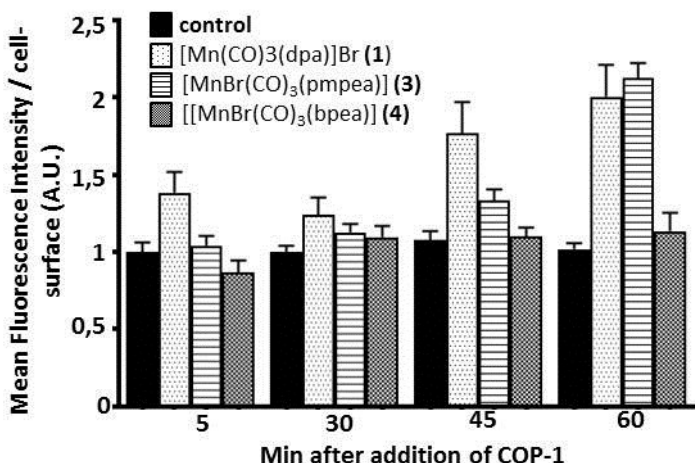


Figure S29. Quantification of CO-release in live HeLa cells at 5, 30, 45 and 60 min after the addition of 1 μM COP-1 in PBS pH 7.4 (lem = 497-558nm ,lex = 488 nm). Cells were previously incubated with either compound (1), (2) or (3) at 150 μM . The results are shown as mean fluorescence intensity (arbitrary units) in relation to the cell-surface area, normalized to control (cells in the absence of compounds). The compounds (1) and (3) show a statistically significant increase in CO-release compared to the control at 45min ((1) $P<0,0001$; (2) $P=0,0012$) and at 60 min ($P<0,0001$), determined by a Mann Whitney test;

Table S1. Calculated and experimental CO stretching frequencies and the λ_{\max} for the proposed structures.

	1		2		3		3 _{py}		4		4 _{py}	
	exp	calc	exp	calc	exp	calc	exp	calc	exp	calc	exp	calc
ν_{sym}	2025	2156	2019	2128	2020	2124	2030	2150	2020	2122	2036	2147
	1935	2098		1914	2072		1910	2066	1939	2089		1905
ν_{asym}	1910	2082			2042		2037	1935	2082		2032	1927
λ_{\max}	350	354	363	391	364	388	362	326	368	397	361	380

Table S2. Selected bond lengths (in Å), where X is the atom in the position trans to a CO. Values inside parenthesis obtained from crystal structure data.

	Bond	Trans to	M-X	M-CO	C-O
1	C(3)-O(3)	N(3)	1.910 (2.058)	1.722 (1.815)	1.170 (1.143)
	C(1)-O(1)	N(1)	1.962 (2.078)	1.704 (1.808)	1.176 (1.146)
	C(2)-O(2)	N(2)	1.909 (2.062)	1.722 (1.803)	1.170 (1.144)
2	C(1)-O(1)	N(1)	1.894 (2.101)	1.713 (1.805)	1.176 (1.146)
	C(2)-O(2)	N(2)	1.972 (2.049)	1.704 (1.803)	1.178 (1.150)
3	C(3)-O(3)	Br(1)	2.421 (2.5238)	1.697 (1.849)	1.185 (1.060)
	C(1)-O(1)	N(14)	1.937 (2.1117)	1.710 (1.811)	1.178 (1.147)
	C(2)-O(2)	N(1)	2.003 (2.1269)	1.703 (1.8044)	1.178 (1.147)
	C(3)-O(3)	Br(1)	2.415 (2.5273)	1.693 (1.8002)	1.186 (1.129)

Table S3. Crystal data and structure refinement for complex 1.

Empirical formula	C ₁₅ H ₁₄ BrMnN ₃ O _{3.50}
Formula weight	427.14
Temperature	200(2) K
Wavelength	0.71073 Å
Crystal system	Monoclinic
Space group	C2/c
Unit cell dimensions	a = 21.6165(7) Å b = 11.8250(3) Å c = 14.9206(5) Å β = 117.8640(10)°
Volume	3371.74(18) Å ³
Z	8
Density (calculated)	1.683 Mg/m ³
Absorption coefficient	3.173 mm ⁻¹
F(000)	1704
Crystal size	0.360 x 0.200 x 0.020 mm ³
Theta range for data collection	2.025 to 30.064°.
Index ranges	-30 ≤ h ≤ 30, -16 ≤ k ≤ 11, -21 ≤ l ≤ 21
Reflections collected	22881
Independent reflections	4947 [R(int) = 0.0365]
Completeness to theta = 25.242°	100.0 %
Absorption correction	Semi-empirical from equivalents
Max. and min. transmission	0.7460 and 0.6140
Refinement method	Full-matrix least-squares on F ²
Data / restraints / parameters	4947 / 0 / 217
Goodness-of-fit on F ²	1.021
Final R indices [I>2sigma(I)]	R1 = 0.0299, wR2 = 0.0610
R indices (all data)	R1 = 0.0510, wR2 = 0.0690
Largest diff. peak and hole	0.682 and -0.426 e.Å ⁻³

Table S4. Bond lengths [\AA] and angles [$^\circ$] for complex **1**.

Mn1-C2	1.803(2)	C5-C6	1.386(3)
Mn1-C1	1.809(2)	N2-C9	1.351(3)
Mn1-C3	1.813(2)	C9-C8	1.376(3)
Mn1-N3	2.0572(15)	C8-C7	1.372(4)
Mn1-N2	2.0624(16)	C7-C6	1.383(4)
Mn1-N1	2.0724(18)	C10-C11	1.496(3)
N1-C10	1.481(3)	C11-N3	1.347(2)
N1-C4	1.485(3)	C11-C12	1.391(3)
C3-O3	1.144(3)	N3-C15	1.344(2)
C1-O1	1.145(3)	C15-C14	1.379(3)
C2-O2	1.144(2)	C14-C13	1.379(3)
C4-C5	1.495(3)	C13-C12	1.379(3)
C5-N2	1.346(3)		
C2-Mn1-C1	88.26(9)	N2-C5-C6	122.1(2)
C2-Mn1-C3	89.78(9)	N2-C5-C4	115.01(17)
C1-Mn1-C3	88.27(10)	C6-C5-C4	122.9(2)
C2-Mn1-N3	89.53(8)	C5-N2-C9	117.96(18)
C1-Mn1-N3	98.23(8)	C5-N2-Mn1	115.45(13)
C3-Mn1-N3	173.44(9)	C9-N2-Mn1	126.43(14)
C2-Mn1-N2	175.47(8)	N2-C9-C8	122.8(2)
C1-Mn1-N2	93.10(8)	C7-C8-C9	118.8(2)
C3-Mn1-N2	94.58(8)	C8-C7-C6	119.4(2)
N3-Mn1-N2	86.00(6)	C7-C6-C5	118.9(2)
C2-Mn1-N1	98.57(8)	N1-C10-C11	111.45(17)
C1-Mn1-N1	173.10(8)	N3-C11-C12	121.51(19)
C3-Mn1-N1	92.65(9)	N3-C11-C10	116.27(17)
N3-Mn1-N1	81.00(7)	C12-C11-C10	122.05(18)
N2-Mn1-N1	80.02(7)	C15-N3-C11	118.45(17)
C10-N1-C4	113.04(17)	C15-N3-Mn1	125.95(13)
C10-N1-Mn1	111.48(13)	C11-N3-Mn1	115.57(13)
C4-N1-Mn1	109.00(13)	N3-C15-C14	122.61(19)
O3-C3-Mn1	176.5(2)	C13-C14-C15	118.9(2)
O1-C1-Mn1	175.8(2)	C14-C13-C12	119.06(19)
O2-C2-Mn1	175.9(2)	C13-C12-C11	119.3(2)
N1-C4-C5	110.05(17)		

Table S5. Torsion angles [°] for complex **1**.

C10-N1-C4-C5	89.5(2)	C4-N1-C10-C11	-101.4(2)
Mn1-N1-C4-C5	-35.09(19)	Mn1-N1-C10-C11	21.8(2)
N1-C4-C5-N2	28.6(2)	N1-C10-C11-N3	-21.3(3)
N1-C4-C5-C6	-153.16(19)	N1-C10-C11-C12	163.34(18)
C6-C5-N2-C9	-1.4(3)	C12-C11-N3-C15	4.0(3)
C4-C5-N2-C9	176.83(17)	C10-C11-N3-C15	-171.35(17)
C6-C5-N2-Mn1	174.18(16)	C12-C11-N3-Mn1	-174.41(15)
C4-C5-N2-Mn1	-7.6(2)	C10-C11-N3-Mn1	10.2(2)
C5-N2-C9-C8	-0.3(3)	C11-N3-C15-C14	-2.8(3)
Mn1-N2-C9-C8	-175.39(16)	Mn1-N3-C15-C14	175.49(14)
N2-C9-C8-C7	1.6(3)	N3-C15-C14-C13	0.1(3)
C9-C8-C7-C6	-1.2(4)	C15-C14-C13-C12	1.2(3)
C8-C7-C6-C5	-0.5(4)	C14-C13-C12-C11	0.0(3)
N2-C5-C6-C7	1.8(3)	N3-C11-C12-C13	-2.7(3)
C4-C5-C6-C7	-176.3(2)	C10-C11-C12-C13	172.42(19)

Table S6. Hydrogen bonds for complex **1** [Å and °].

D-H...A	d(D-H)	d(H...A)	d(D...A)	<(DHA)
O1W-H1W...Br1 ⁱ	0.92	2.39	3.2766(13)	162
C4-H4B...O1W	0.99	2.33	3.254(3)	155
N1-H1...Br1 ⁱⁱ	0.83(3)	2.55(3)	3.3647(19)	170(2)

Symmetry codes: (i) $x+1/2, y+1/2, z$ (ii) $-x+1/2, y+1/2, -z+1/2$

Table S7. Crystal data and structure refinement for complex **3**.

Empirical formula	C ₁₆ H ₁₅ BrMnN ₃ O ₃
Formula weight	432.16
Temperature	200(2) K
Wavelength	0.71073 Å
Crystal system	Monoclinic
Space group	C2/c
Unit cell dimensions	a = 26.1164(8) Å b = 7.3867(2) Å c = 18.3010(6) Å β = 102.9270(10)°
Volume	3441.04(18) Å ³
Z	8
Density (calculated)	1.668 Mg/m ³
Absorption coefficient	3.108 mm ⁻¹
F(000)	1728
Crystal size	0.360 x 0.160 x 0.020 mm ³
Theta range for data collection	1.600 to 30.101°.
Index ranges	-36 ≤ h ≤ 36, -6 ≤ k ≤ 10, -25 ≤ l ≤ 25
Reflections collected	18246
Independent reflections	5051 [R(int) = 0.0316]
Completeness to theta = 25.242°	99.7 %
Absorption correction	Semi-empirical from equivalents
Max. and min. transmission	0.7460 and 0.6251
Refinement method	Full-matrix least-squares on F ²
Data / restraints / parameters	5051 / 0 / 221
Goodness-of-fit on F ²	1.060
Final R indices [I>2sigma(I)]	R1 = 0.0387, wR2 = 0.0880
R indices (all data)	R1 = 0.0600, wR2 = 0.0961
Largest diff. peak and hole	0.636 and -0.525 e.Å ⁻³

Table S8. Bond lengths [Å] and angles [°] for complex 3.

Br1-Mn1	2.5238(4)	N2-C9	1.345(3)
Mn1-C2	1.803(3)	C12-C13	1.392(4)
Mn1-C1	1.805(3)	C12-C11	1.504(4)
Mn1-C3	1.849(3)	C2-O2	1.150(4)
Mn1-N2	2.049(2)	C4-C5	1.499(3)
Mn1-N1	2.101(2)	C5-C6	1.389(3)
O1-C1	1.146(3)	C9-C8	1.379(4)
C3-O3	1.060(3)	C8-C7	1.376(4)
N1-C4	1.481(3)	C7-C6	1.385(4)
N1-C10	1.485(3)	C10-C11	1.535(4)
N3-C16	1.334(4)	C16-C15	1.387(5)
N3-C12	1.343(4)	C15-C14	1.381(5)
N2-C5	1.343(3)	C14-C13	1.369(5)
C2-Mn1-C1	88.48(13)	C9-N2-Mn1	126.20(18)
C2-Mn1-C3	90.20(12)	N3-C12-C13	122.1(3)
C1-Mn1-C3	90.27(11)	N3-C12-C11	116.5(2)
C2-Mn1-N2	174.42(10)	C13-C12-C11	121.4(3)
C1-Mn1-N2	94.59(10)	O2-C2-Mn1	176.8(3)
C3-Mn1-N2	94.44(9)	O1-C1-Mn1	178.8(3)
C2-Mn1-N1	97.73(11)	N1-C4-C5	109.7(2)
C1-Mn1-N1	173.35(10)	N2-C5-C6	122.2(2)
C3-Mn1-N1	92.07(10)	N2-C5-C4	115.5(2)
N2-Mn1-N1	79.03(8)	C6-C5-C4	122.3(2)
C2-Mn1-Br1	89.03(9)	N2-C9-C8	122.0(3)
C1-Mn1-Br1	90.37(8)	C7-C8-C9	119.5(2)
C3-Mn1-Br1	178.98(8)	C8-C7-C6	119.0(2)
N2-Mn1-Br1	86.29(6)	C7-C6-C5	118.7(3)
N1-Mn1-Br1	87.39(6)	N1-C10-C11	114.9(2)
C4-N1-C10	110.9(2)	C12-C11-C10	113.6(2)
C4-N1-Mn1	107.28(15)	N3-C16-C15	123.6(3)
C10-N1-Mn1	118.58(16)	C14-C15-C16	118.5(3)
C16-N3-C12	117.4(2)	C13-C14-C15	118.5(3)
C5-N2-C9	118.5(2)	C14-C13-C12	119.8(3)
C5-N2-Mn1	115.26(15)	O3-C3-Mn1	178.0(3)

Table S9. Torsion angles [°] for complex 3.

C16-N3-C12-C13	2.0(4)	C8-C7-C6-C5	1.8(4)
C16-N3-C12-C11	-178.3(3)	N2-C5-C6-C7	0.6(4)
C10-N1-C4-C5	168.8(2)	C4-C5-C6-C7	-179.4(2)
Mn1-N1-C4-C5	37.8(2)	C4-N1-C10-C11	62.5(3)
C9-N2-C5-C6	-2.8(3)	Mn1-N1-C10-C11	-172.73(19)
Mn1-N2-C5-C6	177.67(18)	N3-C12-C11-C10	-61.6(3)
C9-N2-C5-C4	177.2(2)	C13-C12-C11-C10	118.0(3)
Mn1-N2-C5-C4	-2.3(3)	N1-C10-C11-C12	73.5(3)
N1-C4-C5-N2	-24.5(3)	C12-N3-C16-C15	-0.4(5)
N1-C4-C5-C6	155.5(2)	N3-C16-C15-C14	-1.2(5)
C5-N2-C9-C8	2.6(3)	C16-C15-C14-C13	1.3(5)
Mn1-N2-C9-C8	-177.95(18)	C15-C14-C13-C12	0.2(5)
N2-C9-C8-C7	-0.2(4)	N3-C12-C13-C14	-2.0(4)
C9-C8-C7-C6	-2.0(4)	C11-C12-C13-C14	178.4(3)

Table S10. Crystal data and structure refinement for complex 4.

Empirical formula	C ₁₇ H ₁₇ BrMnN ₃ O ₃
Formula weight	446.18
Temperature	200(2) K
Wavelength	0.71073 Å
Crystal system	Triclinic
Space group	P -1
Unit cell dimensions	a = 8.0271(4) Å b = 9.3057(5) Å c = 12.9921(7) Å α = 87.029(2)° β = 89.037(2)° γ = 67.346(2)°
Volume	894.40(8) Å ³
Z	2
Density (calculated)	1.657 Mg/m ³
Absorption coefficient	2.992 mm ⁻¹
F(000)	448
Crystal size	0.300 x 0.080 x 0.060 mm ³
Theta range for data collection	2.374 to 28.373°.
Index ranges	-10 ≤ h ≤ 10, -12 ≤ k ≤ 12, -17 ≤ l ≤ 17
Reflections collected	15466
Independent reflections	4475 [R(int) = 0.0195]
Completeness to theta = 25.242°	100.0 %
Absorption correction	Semi-empirical from equivalents
Max. and min. transmission	0.8409 and 0.4672
Refinement method	Full-matrix least-squares on F ²
Data / restraints / parameters	4475 / 0 / 230
Goodness-of-fit on F ²	1.042
Final R indices [I>2sigma(I)]	R1 = 0.0235, wR2 = 0.0530
R indices (all data)	R1 = 0.0335, wR2 = 0.0564
Largest diff. peak and hole	0.326 and -0.242 e.Å ⁻³

Table S11. Bond lengths [\AA] and angles [$^\circ$] for complex 4.

Mn1-C3	1.8002(19)	C13-C18	1.392(2)
Mn1-C2	1.8044(19)	N14-C15	1.351(2)
Mn1-C1	1.811(2)	C15-C16	1.374(2)
Mn1-N14	2.1117(13)	C16-C17	1.377(2)
Mn1-N1	2.1269(14)	C17-C18	1.380(2)
Mn1-Br1	2.5273(3)	C21-C22	1.529(3)
C1-O1	1.147(2)	C22-C23	1.509(2)
C2-O2	1.147(2)	C23-N24	1.332(2)
C3-O3	1.129(2)	C23-C28	1.380(3)
N1-C11	1.479(2)	N24-C25	1.338(3)
N1-C21	1.493(2)	C25-C26	1.369(3)
C11-C12	1.522(2)	C26-C27	1.371(3)
C12-C13	1.505(2)	C27-C28	1.383(3)
C13-N14	1.352(2)		
C3-Mn1-C2	90.32(8)	C13-C12-C11	111.47(13)
C3-Mn1-C1	91.41(9)	N14-C13-C18	121.26(15)
C2-Mn1-C1	85.25(9)	N14-C13-C12	118.20(14)
C3-Mn1-N14	91.95(6)	C18-C13-C12	120.39(14)
C2-Mn1-N14	92.58(7)	C15-N14-C13	117.41(14)
C1-Mn1-N14	176.01(8)	C15-N14-Mn1	118.47(11)
C3-Mn1-N1	93.06(7)	C13-N14-Mn1	124.00(11)
C2-Mn1-N1	174.76(7)	N14-C15-C16	123.70(15)
C1-Mn1-N1	90.66(7)	C15-C16-C17	118.91(16)
N14-Mn1-N1	91.30(5)	C16-C17-C18	118.36(16)
C3-Mn1-Br1	178.81(6)	C17-C18-C13	120.35(15)
C2-Mn1-Br1	90.64(6)	N1-C21-C22	114.56(15)
C1-Mn1-Br1	89.37(7)	C23-C22-C21	113.90(15)
N14-Mn1-Br1	87.30(4)	N24-C23-C28	121.70(17)
N1-Mn1-Br1	86.03(4)	N24-C23-C22	116.53(15)
O1-C1-Mn1	175.59(19)	C28-C23-C22	121.76(16)
O2-C2-Mn1	175.43(17)	C23-N24-C25	118.00(17)
O3-C3-Mn1	178.99(17)	N24-C25-C26	123.7(2)
C11-N1-C21	111.13(13)	C25-C26-C27	118.3(2)
C11-N1-Mn1	115.45(10)	C26-C27-C28	118.72(19)
C21-N1-Mn1	115.98(11)	C23-C28-C27	119.56(19)
N1-C11-C12	112.25(14)		

Table S12. Torsion angles [°] for complex **4**.

C21-N1-C11-C12	87.95(17)	C12-C13-C18-C17	-174.71(16)
Mn1-N1-C11-C12	-46.80(16)	C11-N1-C21-C22	74.13(18)
N1-C11-C12-C13	82.32(18)	Mn1-N1-C21-C22	-151.39(12)
C11-C12-C13-N14	-48.8(2)	N1-C21-C22-C23	68.5(2)
C11-C12-C13-C18	126.88(16)	C21-C22-C23-N24	-23.8(2)
C18-C13-N14-C15	-1.9(2)	C21-C22-C23-C28	157.05(18)
C12-C13-N14-C15	173.75(14)	C28-C23-N24-C25	1.3(3)
C18-C13-N14-Mn1	173.92(12)	C22-C23-N24-C25	-177.9(2)
C12-C13-N14-Mn1	-10.4(2)	C23-N24-C25-C26	-0.7(4)
C13-N14-C15-C16	1.5(2)	N24-C25-C26-C27	-0.3(4)
Mn1-N14-C15-C16	-174.58(13)	C25-C26-C27-C28	0.8(4)
N14-C15-C16-C17	0.0(3)	N24-C23-C28-C27	-0.8(3)
C15-C16-C17-C18	-1.1(3)	C22-C23-C28-C27	178.35(19)
C16-C17-C18-C13	0.7(3)	C26-C27-C28-C23	-0.3(3)
N14-C13-C18-C17	0.8(3)		

Table S13. Hydrogen bonds for complex **4** [\AA and °].

D-H...A	d(D-H)	d(H...A)	d(D...A)	\angle (DHA)
N1-H1N...N24	0.83(2)	2.19(2)	2.850(2)	135.7(17)
N1-H1N...Br1	0.83(2)	2.77(2)	3.1885(14)	113.2(16)